Allosteric regulation of glycogen phosphorylase solution phase structural dynamics at high spatial resolution

Monika Kish[a], Victoria Smith[c], Sivaraman Subramanian[b], Frank Vollmer[b], Natasha Lethbridge[c], Lindsay Cole[d], Nick Bond[e], Jonathan James Phillips[a,f,1]

[a] University of Exeter, Living Systems Institute, Department of Biosciences, Exeter EX4 6QD UK [b] University of Exeter, Living Systems Institute, Department of Physics, Exeter EX4 6QD UK [c] Centre for Process Innovation, Darlington UK [d] Applied Photophysics Ltd, Leatherhead UK [e] AstraZeneca Milstein Building, Granta Park, Cambridge CB26 6GH UK [f] Alan Turing Institute, British Library, 96 Euston Road, London NW1 2DB UK

Abstract

Glycogen phosphorylase (GlyP) was the first allosteric enzyme to be described. Yet, the precise dynamic changes in solution phase structure and stability that underpin functional regulation have remained elusive. We have developed a new fully-automated and highly flexible implementation of hydrogen/deuterium-exchange mass spectrometry, operating in the millisecond regime. This enabled measurements of the solution phase local structural dynamics involved in allosteric regulation of GlyP. The sensitivity of these measurements discerned that the 250's loop is natively disordered in the apo T-state, adopting a more ordered conformation in the active state. The quantitative change in stability of the 280s loop is identified, providing the first direct evidence of the entropic switch that sterically regulates substrate access to the active site. Here, we quantify GlyP structural dynamics in solution, describing correlated changes in structure in the activated (pSer14) and inhibited (glucose-6-phosphate bound) forms of the enzyme.

Significance Statement

We have developed a new fully-automated and highly flexible implementation of hydrogen/deuterium-exchange mass spectrometry, operating in the millisecond regime. Measurements of glycogen phosphorylase quantify the solution phase stability of local structure at near-amino acid structural resolution and with no appreciable lower limit of stability. This uncovered the highly-resolved local alterations in stability we provide direct evidence of the entropic mechanism by which access to the active site is gated by the 280s loop.

Introduction

Almost 60 years ago, the term 'allostery' was coined by Monod and Jacob to describe structural and functional regulation of proteins by 'non-steric' means. Yet, the molecular mechanisms for this have remained unclear and hotly debated, with two hypotheses emerging: conformer selection (Monod, Wyman and Changeux) and induced fit (Koshland). Conformer selection is widely observed, where an effector acts by altering the equilibrium (stability) between the active (R) and inactive (T) states. The archetypal allosteric enzyme is glycogen phosphorylase (GlyP) and much insight has been gained from high-resolution structures of trapped R/T-states of GlyP, with seminal work by Barford and co-workers (1), but also from low-resolution studies of enzyme kinetics (2). It remains one of the most widely regulated proteins known, with multiple distinct binding sites for effectors, oligomerization and covalent modification (phosphorylation at Ser14) all contributing to functional modulation.

Now, one open question regarding functional control of GlyP is reflected across much of enzymology: What are the quantitative changes in local Gibbs free energy stability ($\Delta\Delta G$) between R/T-states in solution that underpin allosteric conformer selection(3)(4)(5)? Although GlyP was the first allosteric enzyme to be identified, this is a pivotal and timely question as it is an important and proven therapeutic target for patients with type II diabetes (6), cancers (7) and neurodegenerative diseases (8). Structural biology efforts have revealed a great deal of detail of the alternative postures adopted by GlyP: significantly, some crystallographic models indicated missing density in the 280s loop in the R-state (9GPB.pdb), which condenses to a defined conformation in the T-state (1GPB.pdb)(9, 10). This has been interpreted qualitatively as the critical structural feature to gate

catalytic activity – sterically regulating substrate access to the active site. It remains ambiguous the nature of such a key regulatory mechanism and here we sought to build a quantitative description of this from measurements of the GlyP dimer in solution.

It has been challenging to provide quantitative rationales for the structural switching that is observed in alternately regulated conformations of enzymes, particularly when the molecular size and complexity are large. One such method that can resolve local (near amino acid) perturbations in stability in arbitrarily large proteins is hydrogen/deuterium-exchange mass spectrometry (HDX-MS)(11-16). Moreover, these measurements are made in solution without the need to trap specific conformers, which has been used to answer questions of epitope mapping (17), protein-drug binding (18), protein-protein interactions (19), aggregation (20), effects of mutation (12), and allosteric regulation (21).

Current state-of-the-art HDX-MS systems reproducibly label protein with deuterium during labeling incubation times of approximately 30 seconds or longer, commonly using CTC PAL robotics for automation(22). Recently, there has been growing interest in measuring HDX at the sub-second time-scale to address our inability to measure the structural dynamics and stability of classes of molecule that are currently intractable (including peptide hormones, neurotransmitters and intrinsically disordered proteins/regions)(22, 23). A small number of academic laboratories have reported experimental systems and approaches to obtain millisecond HDX data (24, 25): these include microfluidic chips (26-31), a quench flow apparatus (16, 32) employed for analysis of disordered proteins, a completely online quench flow setup (11)(33) and a capillary mixer for characterizing biological reactions (34, 35).

Here, we describe the construction, validation and implementation of an online flow mixing and quenching system, termed 'ms2min'. With this system we achieved reproducible and repeatable H/D exchange of 50 ms to 300 s. The capability of this instrument to measure accurate, fully-automated and flexible labeling HDX data was determined by studying the stability of synthetic peptides. This validated the approach which was then applied to build a quantitative map of GlyP stability under allosteric activation and inhibition, in solution. To the best of our knowledge, this shows for the first time the precise changes in local stability in response to allosteric modulation, notably in the order/disorder transition of the 280s loop that gates access to the active site.

Results

Fully-automated and flexible pulse-labeling hydrogen/deuterium-exchange mass spectrometry with millisecond precision

Our goal was to quantify the structural switch in solution, along with other coincident dynamic changes in structure between activated (pSer14) and inhibited (glucose-6-phosphate bound) forms of GlyP. To enable this, we developed a fully automated broadband bottom-up HDX-MS approach capable of accurate quantitative assessment of peptide stability. The newly developed ms2min system design (Figure 1A) offers certain significant advances over the other designs previously employed. Notably, it allows fully-automated, software-selection of mixing times over six orders of magnitude (ms to hours) with 1 ms time resolution, flexible labeling temperature control (0 - 25 C), quench temperature control (0 C), on-line connection for 'bottom-up' workflows, two-way communication for reciprocal control of labeling, washing, digestion, desalting and chromatography, automated digestion column wash injection, intercalated blank injections and sample list scheduling of multiple runs.

Precision of D-labeling. To evaluate the measurement variability and labeling precision of the system we determined the repeatability of the quench-flow labeling method. On three separate days we measured the D uptake of 50, 70 and 150 replicates of Bradykinin and Leucine enkephalin at 100 ms mixing time. The short labeling period close to the limit of quantification, was selected as these data points can be very sensitive to variabilities during the labeling reaction. Deviation from the mean value (μ) of each measurement and a histogram of the deviations are shown in Figure 1C. Random, uniform and symmetrical distribution of the deviation from the mean was observed. The daily repeatability standard deviation (SD) computed on day 1, day 2, and on

day 3 was 0.04 Da, 0.04 Da and 0.05 Da for Bradykinin and 0.02 Da, 0.03 Da and 0.02 Da for Leucine Enkephalin. The 95% confidence interval was ±0.01 Da for both Bradykinin and Leucine Enkephalin.

Back exchange is independent of mixing time. The sample experiences different dwell times and flow velocities and characteristics, with respect to different mixing (D-labeling) times. This has the potential to confound attempts to correct for back-exchange, which is required for comparison between proteoforms and for calculation of protection factors. Therefore, we sought to determine whether there is a back-exchange variation with mixing time - specifically, with each different delay loop. The highest measured dependence of back-exchange on mixing time is 0.012% from the linear regression of all five peptides, Figure 1B. In all five peptides, with six different mixing loops that span labeling across four orders of magnitude, no significant correlation could be identified as indicated by the shallow gradient and poor linear correlation coefficient (R^2 <=0.32). The back exchange shows a similar trend between the peptides analyzed by CTC-PAL automation, though the ms2min system preserves more of the deuterium label (Table S3). Therefore, we were able to correct for back exchange within an experiment by reference to a single fully-deuterated sample.

Quantitation of peptide stability

Peptides often have weak protection factors against hydrogen-exchange (36, 37). This renders them intractable by conventional sampling (typically >10 s mixing) as much or even all labeling is complete within the dead-time of the experiment. We sought to determine the extent (i.e. lower limit) to which the ms2min system can quantify peptide stability in solution. We initially chose to measure the stability of synthetic peptides with the ms2min system, as the simple workflow, small datasets and lyophilised samples allow us to validate our approach. Therefore, we collected data for a mixture of three peptides - a hormone (bradykinin), a neurotransmitter (leucine enkephalin), and a consensus sequence antifreeze protein (CN-AFP). The deuterium incorporation was measured at fifteen time points from 0.05 - 300 s and compared with their calculated maximum intrinsic exchange rates (i.e. rate corresponding to a fully unprotected species). The data were corrected for the back- exchange of the system, permitting direct comparison between the measured and theoretical HDX rates in order to obtain protection factors and an estimate of Gibbs free energy stability (ΔG_{ex}) for each peptide. As the observed deuterium incorporation is the sum of a number (q - corresponding to the exchangeable amide groups in the peptide) of exponential exchange rates (k_j), the ideal case would be to fit the data to q exponential phases. This becomes intractable for q>3, given the number of time points that would need to be sampled. Therefore, we fit the data to a stretched exponential function with the fewest phases required to generate a good fit and used this ensemble rate constant to calculate per peptide protection factors (Pf) and stability (G), as previously shown (38).

In each case, there would be no quantitative stability estimate possible under conventional time regimes. We were able to generate good fits to the HDX-MS data automatically and propose Pf and ΔG_{ex} for each peptide (Table 1). Interestingly, Bradykinin is natively disordered in solution, with no protection against maximal theoretical hydrogen exchange rates. All three peptides contained a single amide proton that exchanges even faster than the dead time of this experiment (20 ms), indicating that there is additional information to be gained from faster instrument performance in future.

As the ms2min system is in-line with LC-MS for ‘bottom-up’ experiments, a similar quantitative assessment of peptide stability was then applied to study allosteric regulation of glycogen phosphorylase.

Millisecond HDX-MS of the GlyP dimer.

GlyP forms a dimer of a large (97 kDa) polypeptide chain and so it represents a major challenge to quantitatively link local changes in structure and stability in response to its many regulatory influences. An ms2min-MS approach stands to provide this link, but only if high data density can be achieved, which correlates with high structural resolution and data confidence. For such a large

dataset (three protein conditions each comprising hundreds of individual peptide fragments measured at ten deuterium labeling times, together with theoretical data simulation and global nonlinear regression), it is important that all data acquisition and processing are automated. 273 unique peptides were identified, corresponding to 96.4% sequence coverage (Fig. 2A). In this way, a schedule of ms2min labeling experiments of GlyP - from 50 ms to 30 s - was acquired and analyzed automatically under software control.

Quantitative assessment of local stability in apo-GlyP

We characterized the local stability of GlyP in weakly structured regions (i.e. not the folded core which has HDX half lives > hours) by measuring the structural dynamics in solution at physiologically relevant pH (7.0). Previously it was determined that the subunit interface of the dimer has two main contact regions on opposite sides of the enzyme (1): one between the cap region (residues 35-46) and the α1-α2 loop, β7 and the α2' helix (47-78) of the opposite subunit. The other contact is antiparallel association of the two tower helixes, α7 and immediately adjacent structural elements. The pattern of HDX protection factors matches well to the crystallographic dimer interface (Figure 2B-C) with no additional large protection factors that would indicate tetramer (Fig. S9,S13). The overall level of exchange in apo-GlyP in T-state is very low. This is consistent with a natively folded and rigid enzyme structure.

With a detailed map of local stability in the apo-state of GlyPb, we examined perturbations upon activation/inhibition. The entirely automatic approach from sampling to calculation of peptide-level protection factors (see Materials and Methods) was applied to GlyP in two allosterically regulated states: active GlyPa phosphorylated at Ser14 (pSer14-GlyPa) in the R-state and inactive GlyPb bound to glucose-6-phosphate inhibitor (GlyP:G6P) in the T-state.

Apo GlyP T-state closely resembles GlyP:G6P T-state

Binding of the allosteric inhibitor glucose-6-phosphate (G6P) to the nucleotide allosteric site resulted in only local changes in structure and stability, with some exceptions of long-range minor alterations to helices, α11 and α25 (Fig. S2-10). The G6P interface overlaps the AMP binding site (39), located within the nucleotide allosteric site at a subunit-subunit interface near the C-terminus (Fig. 3). Largest changes in stability were observed for the N-terminus of the α8 helix (-0.45 kcal/mol). Consequently, the C-terminus of α8 and the preceding 280s loop, destabilize by 0.1 kcal/mol. This may represent direct mediation of allostery from the nucleotide site via the rigid α8 helix to the active site, although it is unclear how the partial release of the 280s entropic gate can manifest as inhibitory. The footprint of bound G6P on the polypeptide chain is discernible from the HDX-MS data, yet it is considerably more diffuse than might be anticipated, based on the crystallographic contacts (Fig. S11). Notably, only one inter-chain (van der Waals) contact is identified from the co-crystal structure (between G6P sugar ring around O2 and Val40' of the opposing subunit), yet there is extensive protection against hydrogen-exchange observed throughout the a1'-a2' loop, stabilising those amino acids by -0.25 kcal/mol Fig. 3). This indicates that the loop has considerable conformational flexibility in the apo-form that is significantly constrained by the contacts formed upon ligand binding, namely van der Waals contacts with G6P and with Ile68 and Trp69. Though perhaps expected, no amide hydrogen perturbation is observed in the beta sheet at the rear of the nucleotide site, or in α3, which both consist of extensive H-bonding networks.

Allosteric activation alters local stability throughout the protein

Phosphorylation at the N-terminus (pSer14) induces the well-established flip in local conformation from T-state to R-state. The active and inactive states have notable structural differences, with the major changes known to occur in (i) the catalytic site, (ii) the nucleotide site and (iii) the tower helix (2, 10). We describe the solution phase stability changes in these regions below.

Catalytic site: pSer14-GlyP (GlyPa) exhibits large destabilization extensively throughout the catalytic site (Fig. 4). Largest differences were observed in α6 (+0.37 kcal/mol), β13 (+0.33 kcal/mol) and the β22-α21 loop (+0.33 kcal/mol). Several of these affected amino acids make direct contacts with the pyridoxal phosphate (PLP) cofactor and may contribute to reorientation for

productive catalysis. This allosteric effect is considerably long range: transferring stability from the phosphorylated N-terminus to beyond the PLP around 57 Å.

Tower helix: Upon activation, the tower helix α7 (residues 262-276) alters its angle upwards 10º relative to the long axis of the dimer – increasing solvent accessibility - and unfolds a partial turn into the 250s' loop. This necessarily breaks certain stable contacts with the tower helix' of the other subunit (40). Stability changes are observed in solution consistent with this: the tower helix destabilizes by $\Delta\Delta G_{ex}$ of 0.29 kcal/mol at the N-terminal end (Arg269-Leu271) up to 0.67 kcal/mol at the C-terminal end (Ala272-Ile275). The 250s' loop preceding α7 is found to be natively disordered with an unstable mean ΔG_{ex} in the T-state (+0.95 kcal/mol). However, it is significantly stabilized in GlyPa (ΔG_{ex} -0.30 kcal/mol). The inverse relationship is seen at the other end of the tower helix, in the 280s loop. It was correctly "assumed that 282-286 become mobile" by Barford and co-workers upon transition to the phosphorylated R-state, as the relatively stable loop in the apo T-state (-0.69 kcal/mol) is destabilized by 1.69 kcal/mol (mean average calculated from Pfs that overlap the 280s loop; Fig. S9-10). This provides direct solution phase evidence and quantifies the entropic switch mechanism for the role of the 280s loop in gating access to the catalytic site.

Allosteric sites – The cap' (residues 35-46) and α2 (residues 47-78) interface showed smaller changes than elsewhere in the allosteric transition between GlyPb and GlyPa, however this interface is somewhat stabilized in the active conformation, by an average of -0.29 kcal/mol. The cap' and α2 have been observed to come closer together (40) and we see the solution phase HDX-MS protection is increased in those regions, in line with those conclusions.

Discussion

Structural switching associated with allosteric regulation of enzymes is often predicated on alterations in local stability. This is epitomised in the archetypal allosteric enzyme, glycogen phosphorylase. Access to the GlyP active site is hypothesised to be gated by an order/disorder transition in the 280s loop, constituting an entropic switch. We sought to measure the changes in local structure and stability in GlyP upon allosteric regulation to test this hypothesis and to provide a quantitative basis for the perturbations in solution phase structure.

An automated millisecond hydrogen/deuterium-exchange instrument: Hydrogen exchange rates, under the EX2 regime, can be considered a surrogate of free energy of stability (ΔG_{ex}). However, reliable quantitation of exchange rates requires accurate measurement with deuterium labeling times spanning orders of magnitude – from milliseconds to minutes. We constructed a fully-automated, on-line quench flow instrument ("ms2min") capable of making these measurements in GlyP with flexible labeling with short dead-times and single millisecond resolution. Initial tests on synthetic peptide hormone (bradykinin), neurotransmitter (leucine enkephalin) and consensus anti-freeze protein (CN-AFP) validated the approach by permitting calculation of protection factors, even in natively unstructured regions. The new ms2min system developed here has significant merit from a technical standpoint: huge potential for HDX-MS resolved at the millisecond level has been demonstrated previously, for example applied to the study of protein folding (11) and to TEM lactamase catalysis (15). The ms2min system stands to be particularly impactful in the future study of time-resolved (i.e. non-equilibrium) protein conformational dynamics, given its flexible and high temporal resolution, with software control over single millisecond differences in labeling time, and online full automation.

Apo GlyPb in solution: Apo form GlyP could be seen as a T-state dimer in solution with HDX-MS protection patterns in keeping with the known crystallographic dimer interface. Few changes upon binding of inhibitor, glucose-6-phosphate (G6P) were observed outside of the nucleotide site, confirming that the apo GlyPb resides in a T-state. Just one predicted interaction between G6P and the a1'-a2' loop, at Val40', is sufficient to induce large stabilization in that part of the opposing monomer and gives rise to a diffuse footprint upon inhibitor binding. More direct impact on catalysis was observed as the stability of the 280s loop was reduced, likely via the rigid body helix a8 that experiences the largest stabilizing effect by directly binding to G6P in the nucleotide site. The impact of this change in 280s stability is not immediately clear and warrants further study, but it is

attractive to consider it may be a necessary conflation of the dual use of the nucleotide site which binds to activating and inhibiting allosteric regulators.

Remodelling of the active site in R-state transition: Activation of GlyP by phosphorylation at Ser14 results in large perturbations in the structural ensemble throughout the protein. Although the site of phosphorylation itself, at the N-terminus, was absent in the peptide coverage, the allosteric effects spanned almost 6 nm to the far side of the catalytic site. Multiple loops that contact the pyridoxal phosphate (PLP) cofactor exhibited increased hydrogen-exchange. Much of the solvent accessibility of these loops is via the deep catalytic site itself, which makes it particularly attractive to consider that this dynamic changes result in a reorganisation of PLP orientation in the pocket.

Direct evidence for an entropic switch gating catalytic site access: In the tower helix region – known to traverse the largest geometric changes in the T/R-state transition – the 250' loop is found to be natively disordered in the T-state. This is reciprocally stabilized in concert with the unfolding of the N-terminal turn of the adjacent tower helix (α7). The compensation in stability is even more pronounced at the far (C-terminal) end of the tower helix, where the HDX measurements estimate that the amino acids in the 280s loop are stabilized by between 1.26 and 1.69 kcal/mol. Importantly, the 280s loop is absent in some crystal models of the R-state. This has given rise to the hypothesis that it acts as an entropic switch to gate access to the active site: disordered/unstructured in T-state which blocks glycogen entry; ordered/structured in R-state and held apart by stable contacts with the 250's loop which permits glycogen to access the deep catalytic pocket. Here, we quantitatively confirm this hypothesis by calculating the relative local changes in Gibbs free energy of stability from hydrogen/deuterium-exchange measurements of glycogen phosphorylase dimer in solution.

Materials and Methods

Materials: Glycogen phosphorylase b from rabbit muscle and Glycogen phosphorylase a from rabbit muscle were purchased from Sigma. Chemicals were purchased as follows: potassium phosphate dibasic (99.9%), potassium phosphate monobasic (99.9%), TRIS hydrochloride, Tris(2-carboxyethyl)phosphine hydrochloride (TCEP) and dimethyl sulfoxide-d6 (99.96%) from Sigma; dimethyl sulfoxide (Fisher Bioreagents). Deuterium oxide (99.9% D) was purchased from Goss Scientific. Water, acetonitrile and formic acid (99.5 %) Optima™ LC/MS Grade were from Fisher Scientific. Five peptides were used to prepare the peptide mixture, including Bradykinin (RPPGFSPFR) obtained from Sigma, Leucine enkephalin (YGGFL) from Waters, CN-AFP (DTASDAAAAAALTAANAAAAAEKTAADAAAAAAATAA) from Peptide Synthetics and cTPRH1 (AEAWYNLGNAYYK) and cTPRS (AEAKQNLGNAKQK) were synthesized in-house, as previously described (13). **msHDX system design:** The msHDX system was designed to allow fully automated HDX labeling from the low millisecond to hours time-scale with software control of labeling time, with 1 ms time resolution, temperature control of labeling and quenching and on-line connection to a 2D-chromatography system for conventional 'bottom-up' workflows. **Deuterium-labeling:** All H/D experiments were performed at 23°C labeling temperature in triplicate. The fast mixing system was directly connected to the digestion/separation chamber, however the pepsin column was replaced with a narrow-bore Ti union when the peptides were analyzed.

During the peptide mixture experiments the carrier syringe X contained 20 mM potassium phosphate buffer, pH 7.40 in H_2O. The labeling buffer, 20 mM potassium phosphate buffer at pH 7.06 in D_2O, was placed in the second syringe Y. The mixing ratio in the first mixer was 1:20. Depending on the labeling time, this mixture passed through six different loops at different velocities. The labeling reaction was then rapidly quenched by delivering the quench buffer, 100 mM Potassium phosphate buffer at pH 2.50 in H2O at 0°C degrees into the second mixer, which constituted an approximate 2-fold dilution. The peptide mixture was quenched at 15 time points: 0.05, 0.1, 0.15, 0.20, 0.25, 0.35, 0.5, 0.75, 1, 2.5, 5, 15, 30, 60 and 300 s. The quench buffer was kept in the quench chamber at 0°C degrees in the third syringe Z of the system.

Protein samples were analyzed in triplicate in a completely randomized manner at 9 time points including 0.05, 0.15, 0.25, 0.35, 0.5, 1, 5, 30, and 300 s, with the msHDX instrument as described

above. Digestion was performed online with a pepsin column (Waters). The buffers used while analyzing the protein samples were 40 mM TRIS hydrochloride and 1 mM TCEP at pH 7.00 in H_2O, 40 mM TRIS hydrochloride and 1 mM TCEP at pH 6.60 in D_20 and 100 mM potassium phosphate buffer at pH 2.50 in H_2O, as carrier, labeling and quenching buffers respectively. Data were back exchange corrected with measurements from lyophilized sample resuspended in deuterated pepsin digestion buffer. LC-MS measurements were essentially as previously described (41). **Kinetic analysis.** An in-house Matlab code was developed for automatic calculation of the segment averaged protection factors (Pf) as a measure of the reduced exchange brought by the structure of the protein. The code involves three steps: generating intrinsic uptake curves, fitting them into one- or two stretched exponentials, and plotting and fitting the experimental uptake curves in the same manner. The segment averaged protection factors were estimated by the ratio of the intrinsic exchange rate constant (k_{int}) and measured (experimental) rate constant (k_{exp}). These were used to calculate estimates of Gibbs free energy stability (ΔG_{ex}) and changes in stability ($\Delta\Delta G_{ex}$).

Footnotes

Author contributions: M.K., V.S., S.S., N.L., F.V., N.B., L.C. and J.J.P. designed research; M.K., V.S., S.S., L.C. and J.J.P. performed research; M.K., V.S., S.S., L.C. and J.J.P. analyzed data; and M.K. and J.J.P. wrote the manuscript.

[1]To whom correspondence should be addressed. E-mail: jj.phillips@exeter.ac.uk

Acknowledgements

This work was supported by InnovateUK grant 102612. Applied Photophysics Ltd holds patents covering commercial use of the 'ms2min' instrument. We declare no other financial interests or conflicts of interest.

References

1. Barford D, Johnson LN (1989) The allosteric transition of glycogen phosphorylase. *Nature* 340(6235):609–616.

2. Buchbinder JL, Fletterick RJ (1996) Role of the active site gate of glycogen phosphorylase in allosteric inhibition and substrate binding. *Journal of Biological Chemistry* 271(37):22305–22309.

3. Mueller M, Nidetzky B (2010) Orthophosphate binding at the dimer interface of Corynebacterium callunae starch phosphorylase: mutational analysis of its role for activity and stability of the enzyme. *BMC Biochemistry* 11(1):8.

4. Buller AR et al. (2018) Directed Evolution Mimics Allosteric Activation by Stepwise Tuning of the Conformational Ensemble. *J Am Chem Soc* 140(23):7256–7266.

5. Fan Y, Cross PJ, Jameson GB, Parker EJ (2018) Exploring modular allostery via interchangeable regulatory domains. *Proceedings of the National Academy of Sciences* 115(12):3006–3011.

6. Hoover DJ et al. (1998) Indole-2-carboxamide inhibitors of human liver glycogen phosphorylase. *J Med Chem* 41(16):2934–2938.

7. Zois CE, Harris AL (2016) Glycogen metabolism has a key role in the cancer microenvironment and provides new targets for cancer therapy. *J Mol Med* 94(2):137–154.

8. Brown AM, Ransom BR (2007) Astrocyte glycogen and brain energy metabolism. *Glia* 55(12):1263–1271.

9. Oikonomakos NG, Skamnaki VT, Tsitsanou KE, Gavalas NG, JOHNSON LN (2000) A new allosteric site in glycogen phosphorylase b as a target for drug interactions. *Structure* 8(6):575–584.

10. BARFORD D, Hu SH, JOHNSON LN (1991) Structural mechanism for glycogen phosphorylase control by phosphorylation and AMP. *J Mol Biol* 218(1):233–260.

11. Walters BT, Mayne L, Hinshaw JR, Sosnick TR, Englander SW (2013) Folding of a large protein at high structural resolution. *Proc Natl Acad Sci USA* 110(47):18898–18903.

12. Edgeworth MJ et al. (2015) Global and Local Conformation of Human IgG Antibody Variants Rationalizes Loss of Thermodynamic Stability. *Angew Chem Int Ed Engl* 54(50):15156–15159.

13. Phillips JJ et al. (2017) Rate of Asparagine Deamidation in a Monoclonal Antibody Correlating with Hydrogen Exchange Rate at Adjacent Downstream Residues. *Anal Chem* 89(4):2361–2368.

14. Pan J, Han J, Borchers CH, Konermann L (2012) Structure and Dynamics of Small Soluble A beta(1-40) Oligomers Studied by Top-Down Hydrogen Exchange Mass Spectrometry. *Biochemistry* 51(17):3694–3703.

15. Knox R, Lento C, Wilson DJ (2018) Mapping Conformational Dynamics to Individual Steps in the TEM-1 β-Lactamase Catalytic Mechanism. *J Mol Biol* 430(18 Pt B):3311–3322.

16. Keppel TR, Weis DD (2013) Analysis of Disordered Proteins Using a Simple Apparatus for Millisecond Quench-Flow H/D Exchange. *Anal Chem* 85(10):5161–5168.

17. Deng B et al. (2017) Suppressing allostery in epitope mapping experiments using millisecond hydrogen / deuterium exchange mass spectrometry. *MAbs* 9(8):1327–1336.

18. Klein T et al. (2015) Structural and dynamic insights into the energetics of activation loop rearrangement in FGFR1 kinase. *Nature Communications* 6:7877.

19. Moroco JA et al. (2018) Remodeling of HIV-1 Nef Structure by Src-Family Kinase Binding. *J Mol Biol* 430(3):310–321.

20. Dobson CL et al. (2016) Engineering the surface properties of a human monoclonal antibody prevents self-association and rapid clearance in vivo. *Sci Rep* 6(1):38644.

21. Landgraf RR et al. (2013) Activation of AMP-Activated Protein Kinase Revealed by Hydrogen/Deuterium Exchange Mass Spectrometry. *Structure* 21(11):1942–1953.

22. Coales SJ et al. (2010) Expansion of time window for mass spectrometric measurement of amide hydrogen/deuterium exchange reactions. *Rapid Commun Mass Spectrom* 24(24):3585–3592.

23. Keppel TR, Weis DD (2015) Mapping residual structure in intrinsically disordered proteins at residue resolution using millisecond hydrogen/deuterium exchange and residue averaging. *J Am Soc Mass Spectrom* 26(4):547–554.

24. Resetca D, Wilson DJ (2013) Characterizing rapid, activity-linked conformational transitions in proteins via sub-second hydrogen deuterium exchange mass spectrometry. *FEBS Journal* 280(22):5616–5625.

25. Rob T, Wilson DJ (2012) Time-Resolved Mass Spectrometry for Monitoring Millisecond Time-Scale Solution-Phase Processes. *Eur J Mass Spectrom (Chichester)* 18(2):205–214.

26. Yamamoto T, Shimizu Y, Ueda T, Shiro Y, Suematsu M (2011) Application of micro-reactor chip technique for millisecond quenching of deuterium incorporation into 70S ribosomal protein complex. *International Journal of Mass Spectrometry* 302(1-3):132–138.

27. Resetca D, Wilson DJ (2017) Mapping ligand binding using microfluidics-enabled millisecond timescale hydrogen-deuterium exchange. 420(06):67–73.

28. Rob T, Wilson DJ (2009) A versatile microfluidic chip for millisecond time-scale kinetic studies by electrospray mass spectrometry. *J Am Soc Mass Spectrom* 20(1):124–130.

29. Rob T, Gill PK, Golemi-Kotra D, Wilson DJ (2013) An electrospray ms-coupled microfluidic device for sub-second hydrogen/deuterium exchange pulse-labelling reveals allosteric effects in enzyme inhibition. *Lab Chip* 13(13):2528–2532.

30. Liuni P, Rob T, Wilson DJ (2010) A microfluidic reactor for rapid, low-pressure proteolysis with on-chip electrospray ionization. *Rapid Commun Mass Spectrom* 24(3):315–320.

31. Rob T et al. (2012) Measuring Dynamics in Weakly Structured Regions of Proteins Using Microfluidics-Enabled Subsecond H/D Exchange Mass Spectrometry. *Anal Chem* 84(8):3771–3779.

32. Keppel TR, Howard BA, Weis DD (2012) Addition to Mapping Unstructured Regions and Synergistic Folding in Intrinsically Disordered Proteins with Amide H/D Exchange Mass Spectrometry. *Biochemistry* 51(39):7812–7812.

33. Rist W, Rodriguez F, Jørgensen TJD, Mayer MP (2005) Analysis of subsecond protein dynamics by amide hydrogen exchange and mass spectrometry using a quenched-flow setup. *Protein Science* 14(3):626–632.

34. Konermann L, Wilson DJ (2005) Capillary mixer with adjustable reaction chamber volume for mass spectrometry. *Google Patents*.

35. Zinck N, Stark A-K, Wilson DJ, Sharon M (2014) An Improved Rapid Mixing Device for Time-Resolved Electrospray Mass Spectrometry Measurements. *ChemistryOpen* 3(3):109–114.

36. Bai Y, Milne JS, Mayne L, Englander SW (1993) Primary structure effects on peptide group hydrogen exchange. *Proteins* 17(1):75–86.

37. Bai Y, Milne JS, Mayne L, Englander SW (1994) Protein stability parameters measured by hydrogen exchange. *Proteins* 20(1):4–14.

38. Chetty PS et al. (2009) Helical structure and stability in human apolipoprotein A-I by hydrogen exchange and mass spectrometry. *Proc Natl Acad Sci USA* 106(45):19005–19010.

39. Lorek A et al. (1984) Allosteric interactions of glycogen phosphorylase b. A crystallographic study of glucose 6-phosphate and inorganic phosphate binding to di-imidate-cross-linked phosphorylase b. *Biochemical Journal* 218(1):45–60.

40. Rath VL et al. (2000) Activation of human liver glycogen phosphorylase by alteration of the secondary structure and packing of the catalytic core. *Mol Cell* 6(1):139–148.

41. Stephens AD et al. (2018) Different Structural Conformers of Monomeric α-Synuclein Identified after Lyophilizing and Freezing. *Anal Chem* 90(11):6975–6983.

Figure Legends

Table 1. Calculated segment averaged protection factors.

Figure 1: Characterisation of the fully automated ms2min system. (A) Instrument schematic. Three syringes (E, L and Q) store and deliver the buffers (protonated, deuterated and quenching buffers, respectively), with automated fill/delivery via valves v1-3. Labeling time is varied by matching fluid velocity and the choice of delay loop volume (from six installed loops) prior to mixing with quench. High pressure LC injection valve enables online LC-MS for 'bottom-up' workflows. (B) All labeling times tested exhibit identical back-exchange: the deuterium incorporation observed for fully-deuterated synthetic peptides is invariant with mixing time over more than five orders of magnitude. Linear regression fit with gradient <0.00012 in all cases. (C) Deviation from the mean measurement of deuterium label at 100 ms for Bradykinin and Leucine Enkephalin, n=270 replicate data points with dispersion of 3%. (D) Synthetic peptides exchange at different rates depending on their structure. Absolute hydrogen-exchange (expressed as % deuteration) shown for three peptides compared with theoretical maximum chemical exchange (black dotted curve), error bars denote ±1 r.s.d. from n=3. Stretched exponential fit to experimental data (Red dashed line).

Figure 2: Solution phase local stability and structural perturbation in apo GlyPb dimer. (A) Coverage map of GlyP: 'Bottom-up' hydrogen/deuterium-exchange mass spectrometry relies on spectral assignment of GlyP peptides resulting from pepsin enzyme digest. 273 peptides were

spectrally assigned, corresponding to 95% coverage and redundancy of 4 peptides per amino acid. (B) Heat map indicates the extent of the hydrogen-exchange at each labeling time (rows), given as relative fractional uptake (%). Peptide level data has been averaged per amino acid with linear weighting. (C) Protection factors were calculated from the back-exchange corrected hydrogen exchange rate constants. Up to two protection factors were determined for each peptide (black bars in panel A) which were weighted by the fraction of the peptide exchanging under each regime. Mean average values per amino acid are shown. Gaps in the data were linearly interpolated. Limit of quantitation for slow exchanging peptides was at ln(Pf) = 20. Based on published intrinsic exchange rate constants, an estimate of free energy of stability (ΔG_{ex}) was also calculated (SI fig. 9).

Figure 3: Direct local stabilization of GlyP by binding of glucose-6-phosphate (G6P) to the nucleotide site. The footprint of bound G6P on the polypeptide chain is discernible from the HDX-MS data, yet it is considerably more diffuse than might be anticipated. A large stabilization of -0.25 kcal/mol results in the a1'-a2' loop, even though there is only one contact between G6P and the opposing monomer in the co-crystal structure (SI Fig. 11). HDX data shown for theoretical maximum HDX rate for unstructured polypeptide (black), apo-GlyPb (red), pSer14-GlyPa (blue) and GlyPb:G6P (yellow).

Figure 4: Phosphorylation at Ser14 induces the well-established switch in conformation from T- to R-state. The catalytic site is extensively remodelled upon transition to the R-state by phosphorylation at Ser14 (green spheres). Perturbations in HDX-MS measured rates were detected in several of the loops that contribute to catalytic activity and to pyridoxal phosphate (PLP; purple spheres) binding. local stabilization of GlyP by binding of glucose-6-phosphate (G6P) to the nucleotide site (left panel). The tower helix region appears to behave as an entropic lever with activation inducing stabilization in the 250' loop (at the bottom), slight destabilization in the tower helix (center) and large destabilization in the 280s loop at the entrance to the catalytic site (top). All stability estimates are given in kcal/mol, estimated from HDX-MS rates (see SI). apo-GlyPb (red traces); pSer14-GlyPa (blue traces); GlyPb:G6P (yellow traces); and theoretical maximum HDX rate for unstructured polypeptide (black traces).

Table 1.

Peptide	ln(Pf)		
Bradykinin	-0.42	-0.14	
CN-AFP	1.83		
Leucine Enkephalin	1.79	0.86	-0.15

Figure 1.

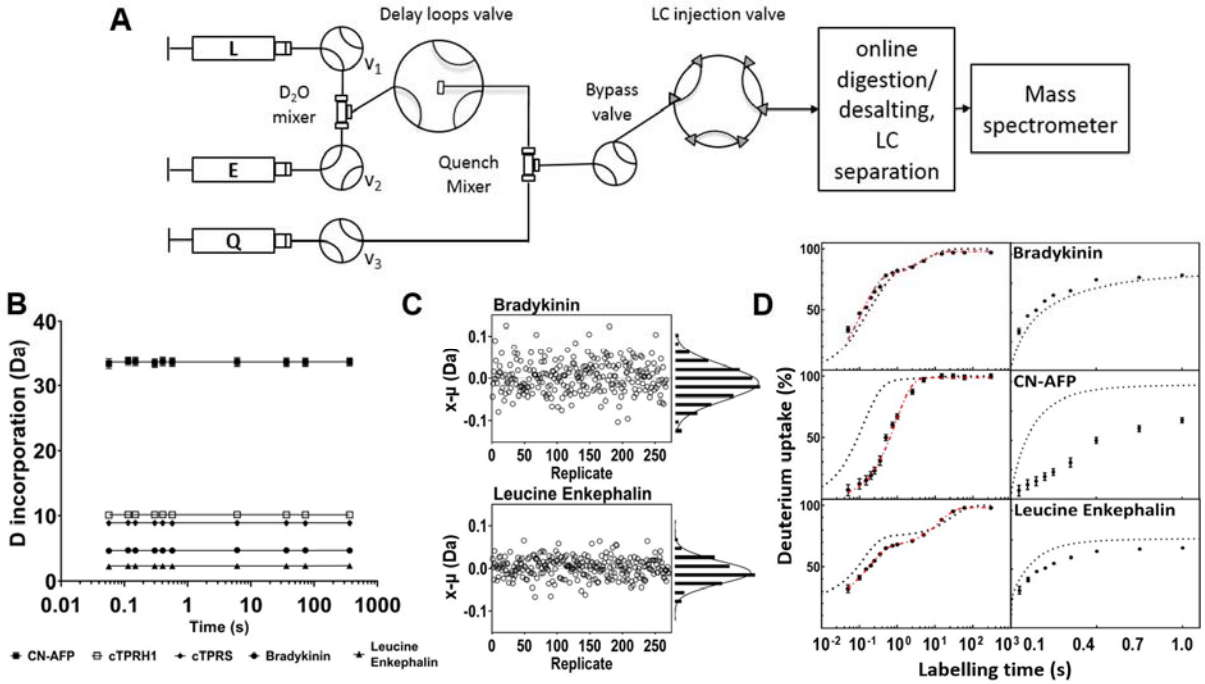
A
Delay loops valve
LC injection valve
L
E
Q
V_1
V_2
V_3
D_2O mixer
Quench Mixer
Bypass valve
online digestion/ desalting, LC separation
Mass spectrometer
B
D incorporation (Da)
Time (s)
CN-AFP
cTPRH1
cTPRS
Bradykinin
Leucine Enkephalin
C
Bradykinin
Leucine Enkephalin
x-μ (Da)
Replicate
D
Bradykinin
CN-AFP
Leucine Enkephalin
Deuterium uptake (%)
Labelling time (s)

Figure 2.

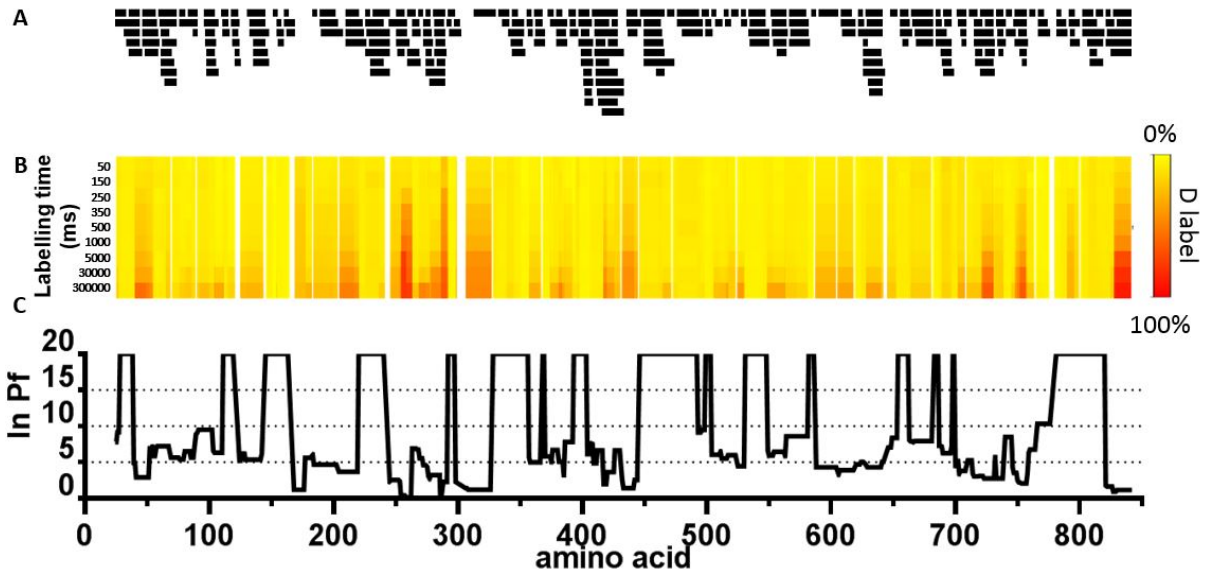
A
B
Labelling time (ms)
50
150
250
350
500
1000
5000
30000
300000
0%
D label
100%
C
ln Pf
20
15
10
5
0
0
100
200
300
400
500
600
700
800
amino acid

Figure 3.

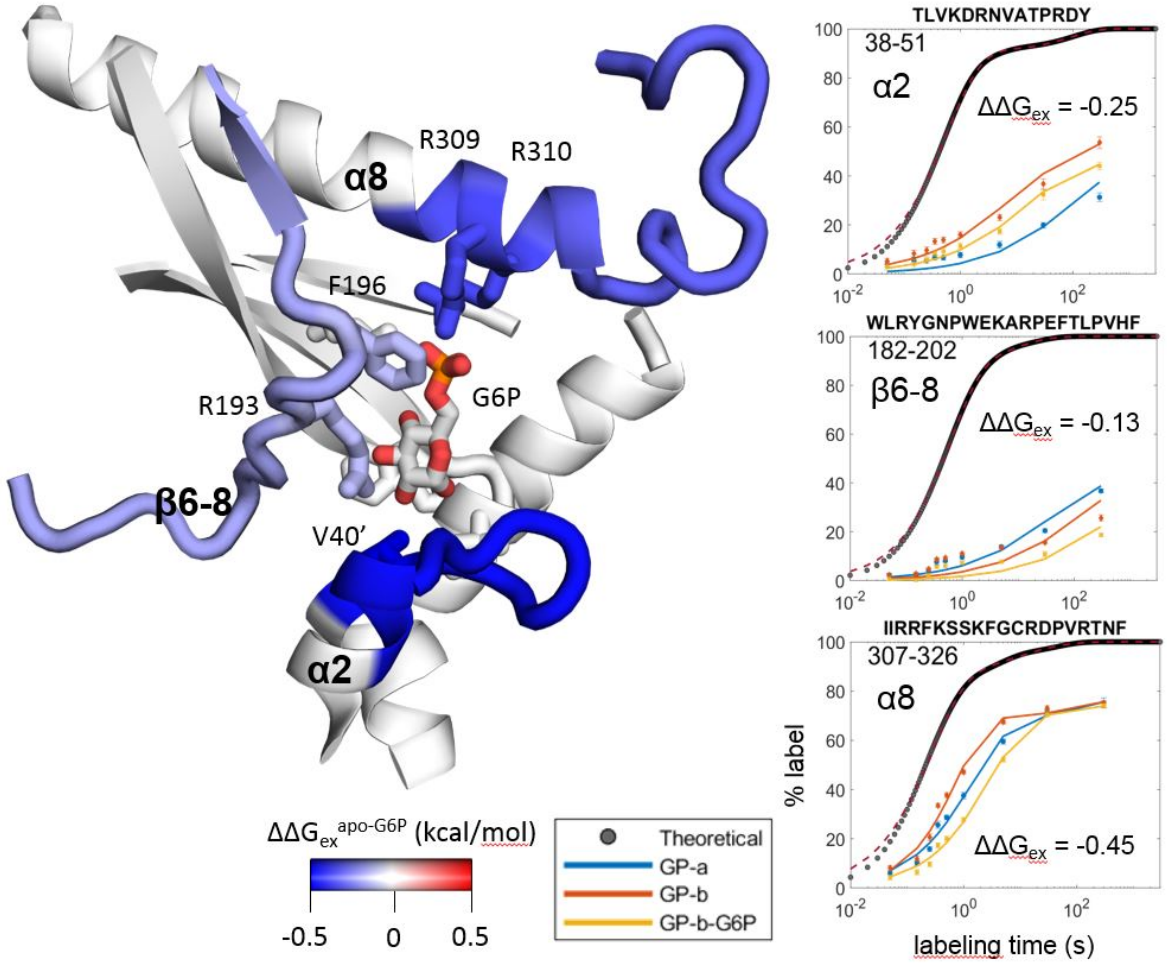
R309
R310
α8
F196
R193
G6P
β6-8
V40'
α2
ΔΔG_ex^apo-G6P (kcal/mol)
-0.5
0
0.5
Theoretical
GP-a
GP-b
GP-b-G6P
TLVKDRNVATPRDY
38-51
α2
ΔΔG_ex = -0.25
WLRYGNPWEKARPEFTLPVHF
182-202
β6-8
ΔΔG_ex = -0.13
IIRRFKSSKFGCRDPVRTNF
307-326
α8
ΔΔG_ex = -0.45
% label
labeling time (s)

Figure 4.

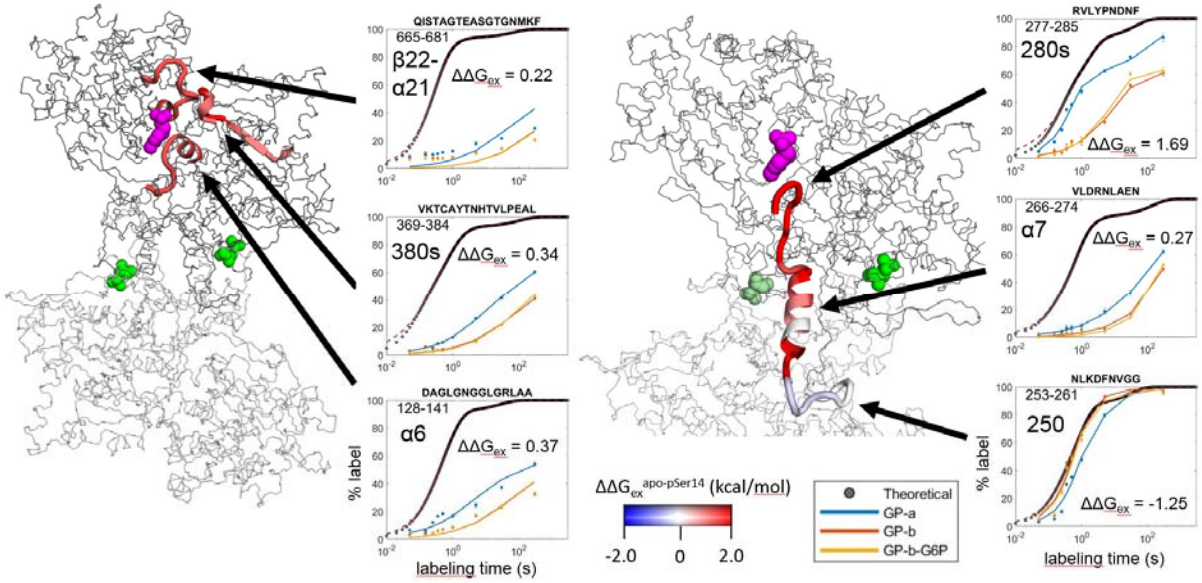
QISTAGTEASGTGNMKF
665-681
β22-
α21
ΔΔG_ex = 0.22
VKTCAYTNHTVLPEAL
369-384
380s
ΔΔG_ex = 0.34
DAGLGNGGLGRLAA
128-141
α6
ΔΔG_ex = 0.37
% label
labeling time (s)
ΔΔG_ex^apo-pSer14 (kcal/mol)
-2.0
0
2.0
Theoretical
GP-a
GP-b
GP-b-G6P
RVLYPNDNF
277-285
280s
ΔΔG_ex = 1.69
VLDRNLAEN
266-274
α7
ΔΔG_ex = 0.27
NLKDFNVGG
253-261
250
ΔΔG_ex = -1.25
% label
labeling time (s)

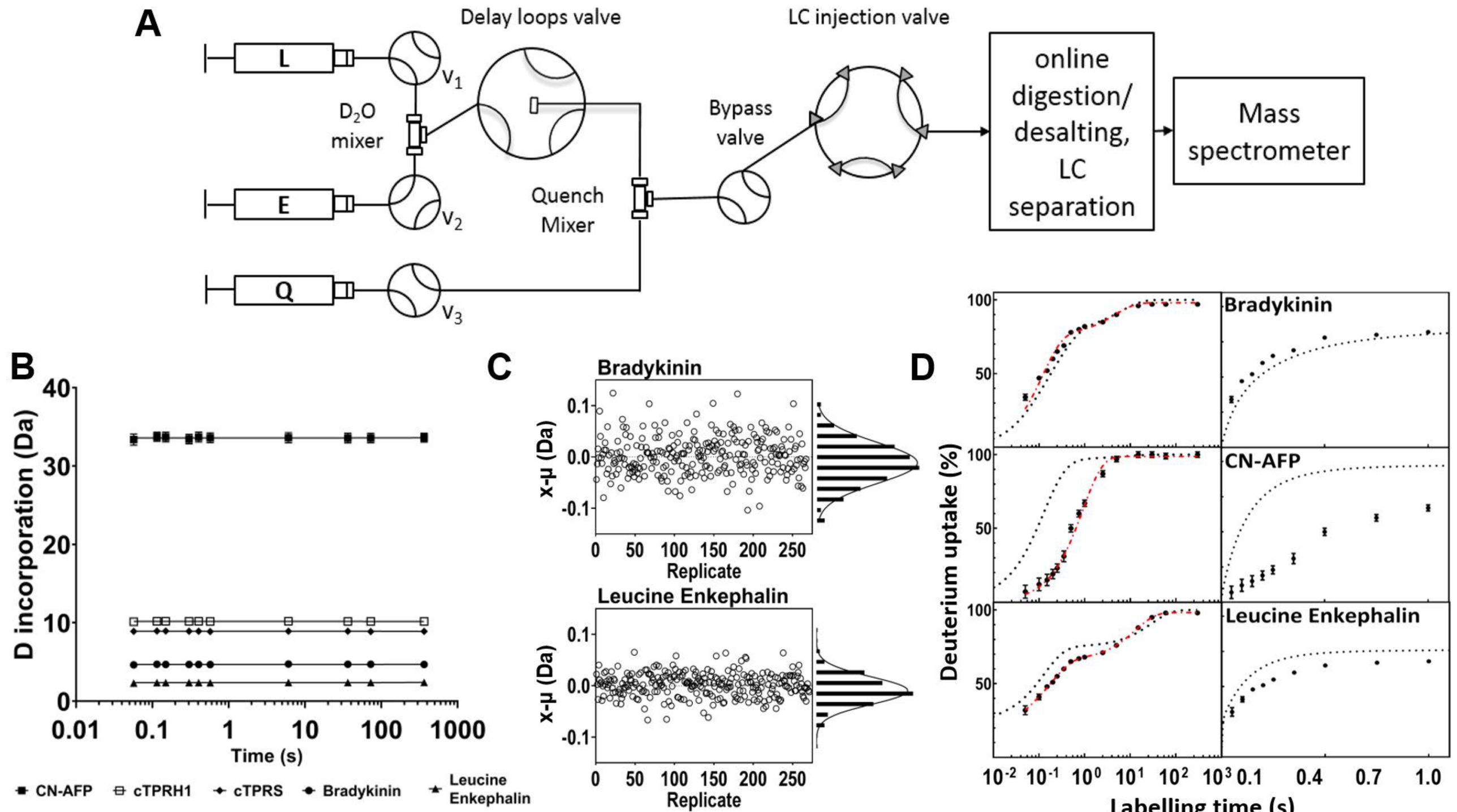
A
Delay loops valve
LC injection valve
L
E
Q
V1
V2
V3
D2O mixer
Quench Mixer
Bypass valve
online digestion/ desalting, LC separation
Mass spectrometer
B
D incorporation (Da)
Time (s)
CN-AFP
cTPRH1
cTPRS
Bradykinin
Leucine Enkephalin
C
Bradykinin
Leucine Enkephalin
x-μ (Da)
Replicate
D
Deuterium uptake (%)
Labelling time (s)
Bradykinin
CN-AFP
Leucine Enkephalin

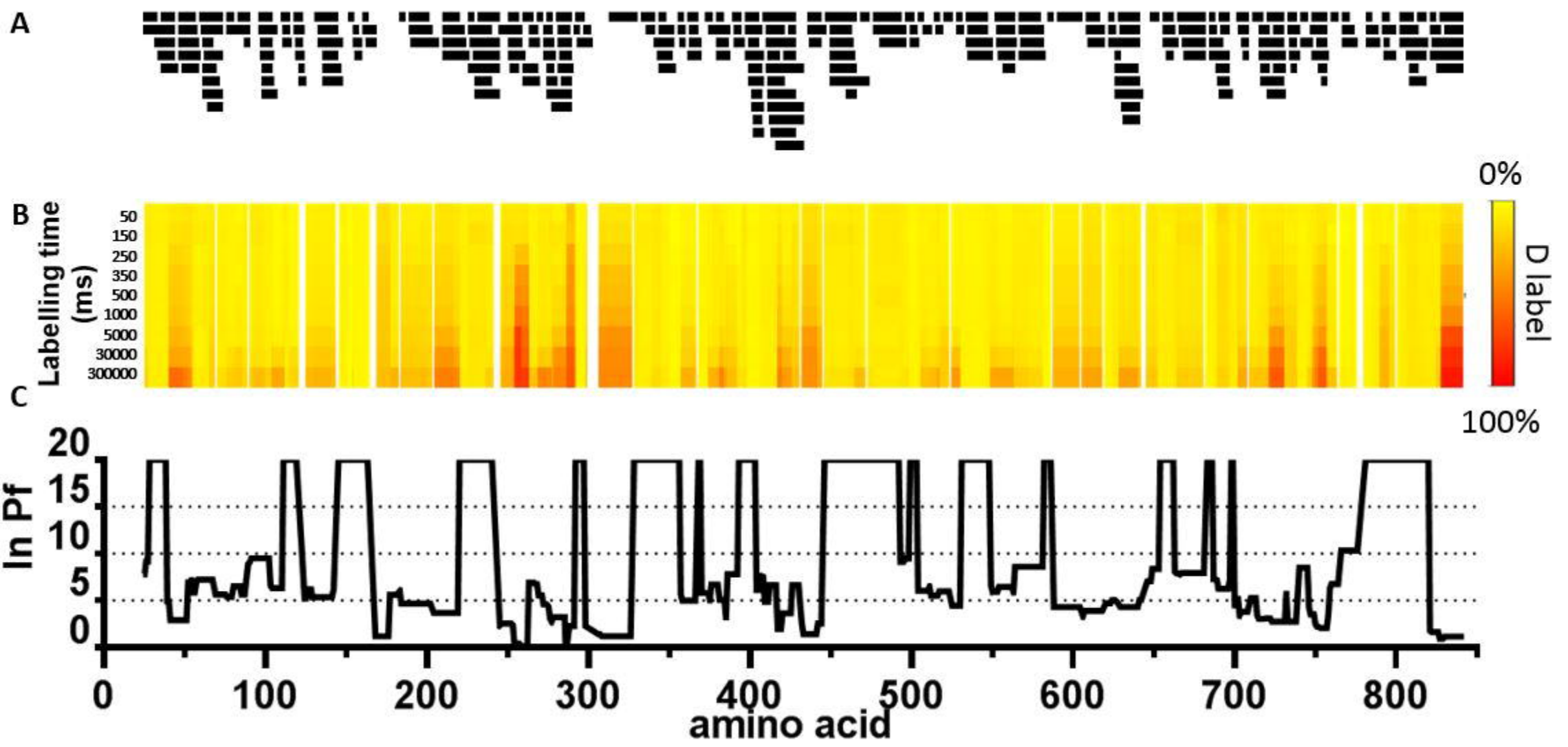
A
B
Labelling time (ms)
50
150
250
350
500
1000
5000
30000
300000
0%
D label
100%
C
ln Pf
20
15
10
5
0
0
100
200
300
400
500
600
700
800
amino acid

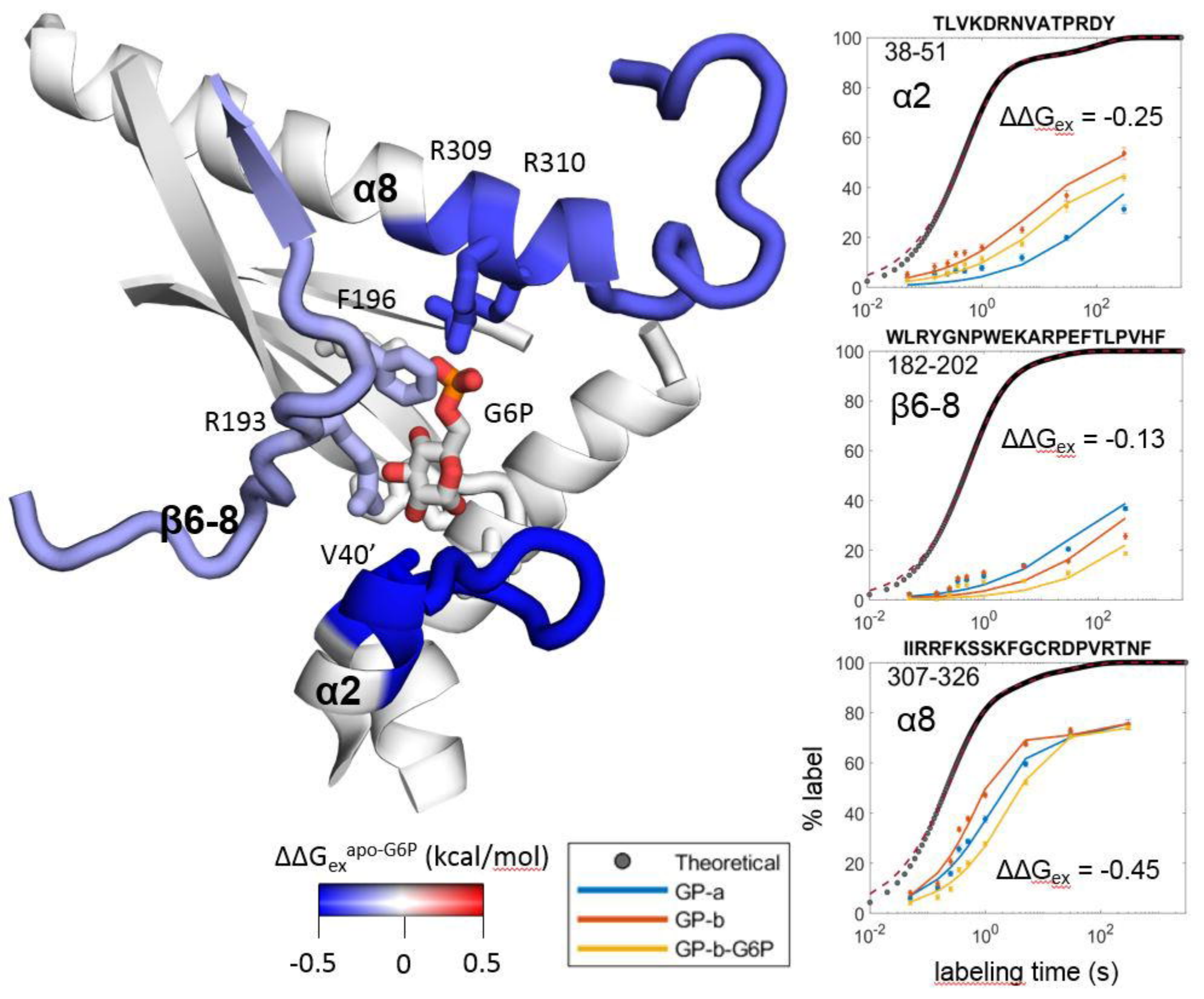
R309
R310
α8
F196
R193
G6P
β6-8
V40'
α2
ΔΔG_ex^apo-G6P (kcal/mol)
-0.5
0
0.5
Theoretical
GP-a
GP-b
GP-b-G6P
TLVKDRNVATPRDY
38-51
α2
ΔΔG_ex = -0.25
WLRYGNPWEKARPEFTLPVHF
182-202
β6-8
ΔΔG_ex = -0.13
IIRRFKSSKFGCRDPVRTNF
307-326
α8
ΔΔG_ex = -0.45
% label
labeling time (s)

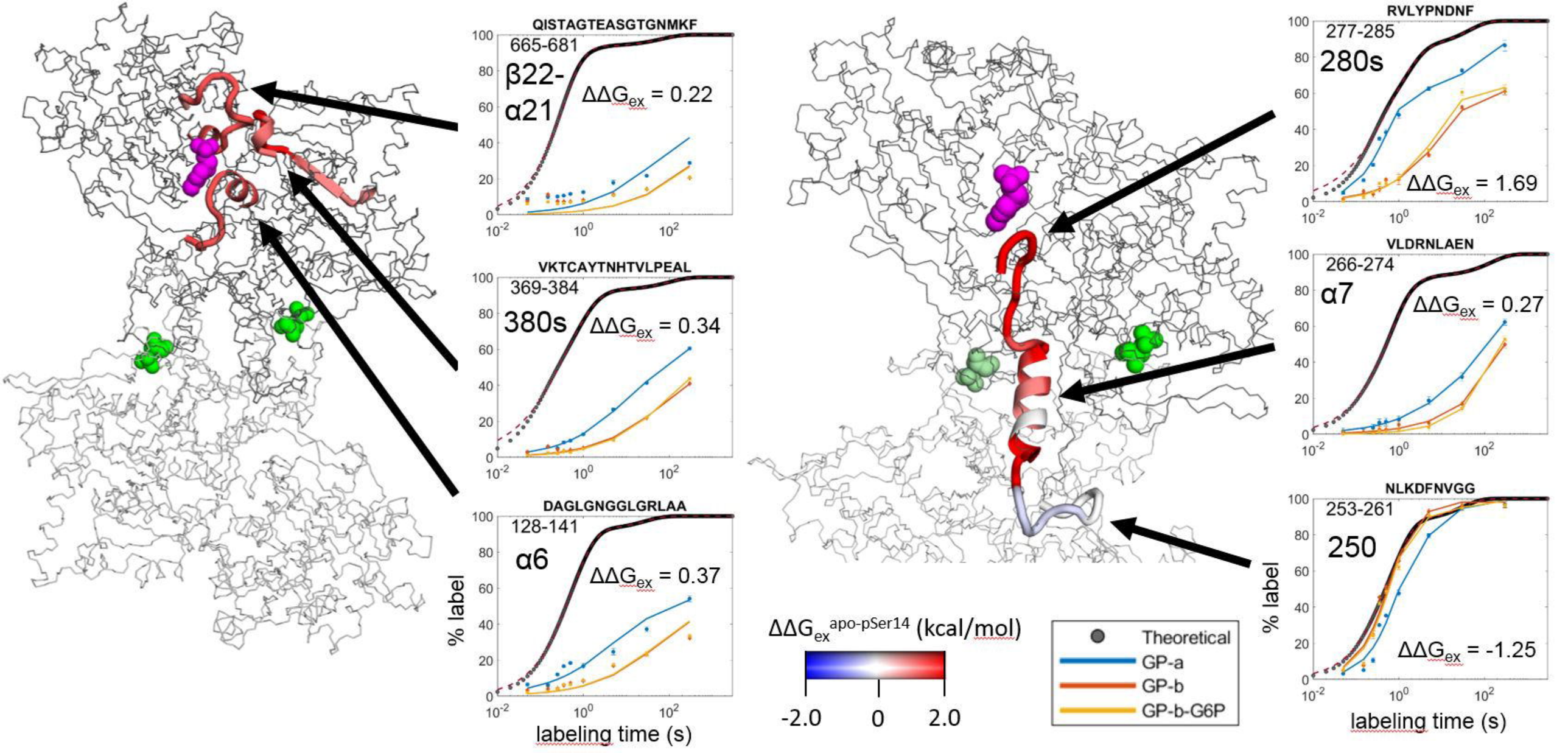
QISTAGTEASGTGNMKF
665-681
β22-α21
ΔΔG_ex = 0.22
VKTCAYTNHTVLPEAL
369-384
380s
ΔΔG_ex = 0.34
DAGLGNGGLGRLAA
128-141
α6
ΔΔG_ex = 0.37
% label
labeling time (s)
RVLYPNDNF
277-285
280s
ΔΔG_ex = 1.69
VLDRNLAEN
266-274
α7
ΔΔG_ex = 0.27
NLKDFNVGG
253-261
250
ΔΔG_ex = -1.25
% label
labeling time (s)
ΔΔG_ex^apo-pSer14 (kcal/mol)
-2.0
0
2.0
Theoretical
GP-a
GP-b
GP-b-G6P